



1 **The use of radiocarbon ^{14}C to constrain carbon dynamics in the soil module**
2 **of the land surface model ORCHIDEE (SVN r5165)**
3
4

5 **Marwa Tifafi¹, Marta Camino-Serrano^{2,3}, Christine Hatté¹, Hector Morras⁴, Lucas**
6 **Moretti⁵, Sebastián Barbaro⁵, Sophie Cornu⁶, Bertrand Guenet¹**

7
8 ¹Laboratoire des Sciences du Climat et de l'Environnement, LSCE/IPSL, CEA-CNRS-UVSQ,
9 Université Paris-Saclay, F-91191 Gif-sur-Yvette, France.

10 ²CREAF, Cerdanyola del Vallès, 08193, Catalonia, Spain

11 ³CSIC, Global Ecology Unit CREAF-CSIC-UAB, Bellaterra 08193, Catalonia, Spain

12 ⁴INTA-CIRN, Instituto de Suelos, 1712 Castelar, Buenos Aires, Argentina

13 ⁵INTA-EEA Cerro Azul, 3313 Cerro Azul, Misiones, Argentina

14 ⁶Aix Marseille Univ, CNRS, IRD, INRA, Coll France, CEREGE, Aix-en-Provence, France

15

16 Corresponding authors: Marwa Tifafi (marwa.tifafi@lsce.ipsl.fr)

17

18 **Abstract.** Despite the importance of soil as a large component of the terrestrial ecosystems, the
19 soil compartments are not well represented in the Land Surface Models (LSMs). Indeed, soils
20 in current LSMs are generally represented based on a very simplified schema that can induce a
21 misrepresentation of the deep dynamics of soil carbon. Here, we present a new version of the
22 IPSL-Land Surface Model called ORCHIDEE-SOM, incorporating the ^{14}C dynamic in the soil.
23 ORCHIDEE-SOM, first, simulates soil carbon dynamics for different layers, down to 2 m
24 depth. Second, concentration of dissolved organic carbon (DOC) and its transport are modeled.
25 Finally, soil organic carbon (SOC) decomposition is considered taking into account the priming
26 effect.

27 After implementing the ^{14}C in the soil module of the model, we evaluated model outputs against
28 observations of soil organic carbon and ^{14}C activity ($F^{14}\text{C}$) for different sites with different
29 characteristics. The model managed to reproduce the soil organic carbon stocks and the $F^{14}\text{C}$
30 along the vertical profiles. However, an overestimation of the total carbon stock was noted, but
31 was mostly marked on the surface. Then, thanks to the introduction of ^{14}C , it has been possible
32 to highlight an underestimation of the age of carbon in the soil. Thereafter, two different tests
33 on this new version have been established. The first was to increase carbon residence time of
34 the passive pool and decrease the flux from the slow pool to the passive pool. The second was
35 to establish an equation of diffusion, initially constant throughout the profile, making it vary
36 exponentially as a function of depth. The first modifications did not improve the capacity of the
37 model to reproduce observations whereas the second test showed a decrease of the soil carbon
38 stock overestimation, especially at the surface and an improvement of the estimates of the
39 carbon age. This assumes that we should focus more on vertical variation of soil parameters as
40 a function of depth, mainly for diffusion, in order to upgrade the representation of global carbon
41 cycle in LSMs, thereby helping to improve predictions of the future response of soil organic
42 carbon to global warming.



43 **1 Introduction**

44 The complexity of the mechanisms involved in controlling soil activity (Jastrow et al., 2007)
45 and therefore the carbon flux from the soil to the atmosphere makes predicting the response of
46 these systems to climate change extremely complex. Thus our ability to predict future changes
47 in carbon stocks in soils using global climate models of the processes governing storage and
48 destocking at variable time and space scales is currently heavily criticized (Todd-Brown et al.,
49 2013; Wieder et al., 2013). Indeed, Earth System Models (ESMs) are increasingly used today
50 in order to predict the future evolution of the climate. For instance, results of a set of ESMs are
51 taken into account within the Intergovernmental Panel on Climate Change (IPCC) (Taylor et
52 al., 2012) for assessment of the impacts of climate change and design of mitigation strategies.
53 Hence, their predictions need to be as accurate as possible. These models represent the physical,
54 chemical and biological processes within and between the atmosphere, ocean and terrestrial
55 biosphere. They allow us to follow and understand, on the one hand the effect of the climate on
56 carbon and vegetation and vice versa. However, ESMs are currently under development and
57 some key processes in the global carbon cycle are still missing or not represented with the
58 necessary details. One of the components of the ESMs is the land surface model (LSM). This
59 component primarily manages the carbon cycle, energy and water on land and simulate the
60 carbon uptake by plants between the atmosphere and the land, namely the gross primary
61 production (GPP) and heterotrophic soil respiration.

62 Despite the importance of soils as a large component of the global carbon storage, the soil
63 compartments are not well represented in LSMs (Todd-Brown et al., 2013). Indeed, carbon
64 dynamics in soil described in LSMs are founded on the model “Century” (Parton et al., 1987)
65 or the Roth-C model (Coleman et al., 1997) where soil carbon is represented as several pools,
66 with different turnover rates for each pool. Carbon is decomposed in each pool, one part is then
67 transferred from one pool to another and the other part is lost through heterotrophic respiration.
68 In addition, soils are generally represented as a single-layer box in LSMs that do not take into
69 account the evolution and variation of soil organic processes as a function of depth (Todd-
70 Brown et al., 2013).

71 One way to reconcile this simplified representation of carbon dynamics of the models with the
72 complexity of the data collected in the field is to integrate isotopic tracers into the models
73 themselves and thus to facilitate the comparison between model outputs and data (He et al.,
74 2016). Indeed, in order to be more pertinent in evaluating the parameters and the equations of
75 the newly implemented processes, it is of interest implementing carbon isotope dynamics in the
76 model itself, this to facilitate the comparison between model outputs and available observations,
77 but also, thanks to an additive constraints on the model structure, to improve the model
78 performances. For instance, radiocarbon is an important tool for studying the dynamics of soil
79 organic matter (Trumbore, 2000). Indeed, ^{14}C acquired on soil organic matter, provide
80 complementary information on the dynamics (temporal dimension) of soil organic matter. This
81 tracer have the major advantage of being integrator of carbon dynamics on long time scales (a
82 few decades to several centuries). It is therefore a very powerful tool to constrain conceptual
83 schemes that may not be directly compared to variables measured in the field because of the
84 conceptual description by pools non measurable (Elliott et al., 1996).



85 First, there is the natural radiocarbon produced at a constant rate in the upper atmosphere during
86 the bombardment of cosmic rays. Thus it provides information on the dynamics of organic
87 matter that has been stabilized by interaction with mineral surfaces and then been stored long
88 enough for significant radioactive decay (Trumbore, 2000) since the half-life of ^{14}C is about
89 5730 years. Then, we distinguish the radiocarbon produced during the atmospheric tests of
90 thermonuclear weapons in the early sixties which act as tracer thanks to the bomb peak of the
91 1960s (Delibrias et al., 1964; Hua et al., 2013). Atmospheric bomb testing in the late 1950's and
92 early 1960's yielded for the abrupt increase of atmospheric ^{14}C concentration that doubles in 2-
93 3 years. By exchange with ocean and terrestrial reservoirs, it decreases since but still remains
94 above the natural background. As any other carbon isotopes, this ^{14}C was metabolized by the
95 vegetation and transferred to soil. By measuring ^{14}C activity of soil sample and looking at the
96 high values, it is possible to evaluate the amount of carbon introduced into the soil since the
97 1960s (Balesdent and Guillet, 1982; Scharpenseel and Schiffmann, 1977).

98 In this study, we present a new version of the IPSL-Land Surface Model called ORCHIDEE-
99 SOM incorporating the ^{14}C dynamic in the soil. Thanks to this tracer, we evaluate the SOC
100 dynamics, in particular by looking at the ^{14}C peak produced by atmospheric weapons testing
101 and observed in the soils at four different sites having different biomes.

102

103 **2 Materials and methods**

104 **2.1 ORCHIDEE-SOM overview**

105 ORCHIDEE is the Land Surface Model of the IPSL (Institut Pierre Simon Laplace) Earth
106 System Model (Krinner et al., 2005). It is composed of three different modules. First, SECHIBA
107 (Ducoudré et al., 1993; de Rosnay and Polcher, 1998), the Surface-vegetation-atmosphere
108 transfer scheme, describing the soil water budget and energy and water exchanges. The time
109 step of this module is 30 min. Second, module of the vegetation dynamics which has been taken
110 from the dynamic global vegetation model LPJ (Sitch et al., 2003). The time step of this module
111 is 1 year. Finally, STOMATE (Saclay Toulouse Orsay Model for the Analysis of Terrestrial
112 Ecosystems) module which essentially simulates the phenology and carbon dynamics with a
113 time step of 1 day.

114 ORCHIDEE can be run coupled to a global circulation model. However, since our study focuses
115 on changes in the land surface rather than on the interaction with climate, we run ORCHIDEE
116 on off line configuration. In this case, the atmospheric conditions such as temperature, humidity
117 and wind are read from meteorological dataset. The climate data CRUNCEP used for our study
118 (6-hourly climate data over several years) were obtained from the combination of two existing
119 datasets: the Climate Research Unit (CRU) (Mitchell et al., 2004) and the National Centers for
120 Environmental Prediction (NCEP) (Kalnay et al., 1996).

121 Our starting point is the ORCHIDEE-SOM version, based on the SVN r3340 version (Krinner
122 et al., 2005), which is presented in details in Camino-Serrano et al. (2017). Figure 1 represents
123 how the soil is described in this new version. Indeed, the major particularity of ORCHIDEE-
124 SOM is that it simulates the dynamics of soil carbon for 11 layers from the surface to 2 m depth.
125 First, litter is divided into four pools: metabolic or structural litter pools which can be found



126 below or aboveground. Only the belowground litter is modeled on 11 horizons, from surface to
 127 2 m depth, however, the aboveground litter layer has a fixed thickness, 10 mm. Second, SOC
 128 is divided into three pools (active, passive and slow), following Parton et al. (1988), which
 129 differ in their turnover rates and which are discretized into 11 layers up to two meters. Then,
 130 dissolved organic carbon (DOC) is represented as two pools also discretized into 11 layers up
 131 to two meters: the labile DOC with a high decomposition rate and the recalcitrant DOC with a
 132 low decomposition rate (Camino-Serrano et al., 2017). Finally, another particularity of this
 133 version of ORCHIDEE-SOM is that the SOC decomposition is modified to account for the
 134 priming effect following Guenet et al. (2016).

135 Since the soil profile is divided into 11 layers, SOC and DOC transport following the diffusion
 136 is also described. SOC diffusion is actually a representation of bioturbation processes (animal
 137 (and plant) activity), whereas DOC diffuses through concentration gradients.

138 This is represented using the Fick's law (Braakhekke et al., 2011; Elzein and Balesdent, 1995;
 139 O'Brien and Stout, 1978; Wynn et al., 2005):

$$140 \quad F_D = -D * \frac{\partial^2 C}{\partial z^2} \quad (1)$$

141 Where F_D is the flux of carbon transported by diffusion in $\text{g C m}^{-3} \text{ day}^{-1}$, D is the diffusion
 142 coefficient ($\text{m}^2 \text{ day}^{-1}$) and C is the amount of carbon in the pool (DOC or SOC) subject to
 143 transport (g C m^{-3}). The diffusion coefficient is assumed to be constant across the soil profile
 144 in ORCHIDEE-SOM but the diffusion parameters (D) used in the equations for SOC and DOC
 145 are different.

146 2.2 ORCHIDEE-SOM- ^{14}C

147 In ORCHIDEE-SOM, the different compartments (soil carbon input, litter, SOC, DOC and
 148 heterotrophic respiration) are presented as matrix with a single dimension referring to the total
 149 carbon. In order to introduce the ^{14}C , a new dimension has been added to all the variables cited
 150 above. Thus, all processes that apply to the total soil carbon are now also represented for ^{14}C .
 151 This new version including the ^{14}C will be called ORCHIDEE-SOM- ^{14}C .

152 Several ways of reporting ^{14}C activity levels are available. We chose to use the *fraction modern*,
 153 with the $F^{14}\text{C}$ symbol as advocated by Reimer et al. (2004) rather than absolute concentration
 154 of ^{14}C (that should be reported as Bq).

$$155 \quad F^{14}\text{C} = \left(\frac{A_S}{0.95 A_{OX1}} \right) * \left(\frac{0.975}{0.981} \right)^2 * \left[\left(1 + \frac{\delta^{13}C_{OX1}}{1000} \right) / \left(1 + \frac{\delta^{13}C_S}{1000} \right) \right]^2 \quad (2)$$

156 with $A = ^{14}\text{C}/^{12}\text{C}$, S for sample, OX1 for Oxalic Acid 1, the ^{14}C international standard.
 157 $F^{14}\text{C}$ is twice normalized: i- it takes into account isotopic fractionation by being normalized to
 158 a $\delta^{13}\text{C} = -25\text{‰}$ and ii- it corresponds to a deviation towards an international standard (i.e. 95%
 159 of OX1 as measured in 1950 – (Stuiver and Polach, 1977)). By propagating $F^{14}\text{C}$ from
 160 atmosphere at the origin of vegetal photosynthesis to soil respired CO_2 , there is no need to focus
 161 on ^{13}C isotopic fractionation all along the organic matter mineralization with $F^{14}\text{C}$.

162 To make easier the reading of the paper, we will further expressed $F^{14}\text{C}$ as $F^{14}\text{C} = A_{\text{sample}}/A_{\text{ref}}$
 163 with normalizations included into A_{ref} and to simplify the notation with superscript and
 164 subscript $F^{14}\text{C}$ will be restricted to F^{14} .



165 Since we focus on SOC dynamics, we did not include the ^{14}C in the plants but directly in the
 166 litter. The ^{14}C -litter is obtained by multiplying by F (atmospheric value) the total carbon's litter:

$$167 \quad Litter(carbon14) = F_{atm}^{14} * Litter(carbon) \quad (3)$$

168 where F_{atm}^{14} is the $F^{14}\text{C}$ of atmosphere at the time of leaf growth (figure 2).

169 Thus, from the litter, all processes defined in section 2.1 that apply to total soil carbon are also
 170 represented for ^{14}C .

171 We also take into account the radioactive decay of ^{14}C . For that, we calculate the amount of ^{14}C
 172 as follow:

$$173 \quad carbon14 = carbon14 - K_{decrease} * carbon14 \quad (4)$$

174 Where $k_{decrease}$ is the radioactive decay constant ($=\text{Ln}2/5730$) (Godwin, 1962)

175 Then, $F^{14}\text{C}$ of the soil is calculated back for carbon, per pool:

$$176 \quad F_{Pool,z}^{14} = \frac{Carbon14_{Pool,z}}{Carbon_{Pool,z}} \quad (5)$$

177 with pool representing the active, slow or passive pool.

178 So finally, we calculate a mean $F^{14}\text{C}$ value per soil, according to the depth:

$$179 \quad F_{Mean,z}^{14} = \frac{F_{active,z}^{14} * Carbon14_{active,z} + F_{slow,z}^{14} * Carbon14_{slow,z} + F_{passive,z}^{14} * Carbon14_{passive,z}}{Carbon14_{active,z} + Carbon14_{slow,z} + Carbon14_{passive,z}} \quad (6)$$

180 2.3 Sites description

181 2.3.1 French sites

182 Two Luvisol (WRB, 2006) (profiles located in the northern France were selected: Feucherolles
 183 and Mons sites. In Mons (49.87°N, 3.03°E), Luvisol, under grassland, are developed from
 184 several meters of loess and are thus well drained. The mean annual air temperature is 11°C and
 185 the annual precipitation is about 680 mm (Keyvanshokouhi et al., 2016). In Feucherolles, under
 186 oaks forest, site (48.9°N, 1.97°E), clay and gritstone deposits are found at approximately 1.5m
 187 depth. The mean annual air temperature is 11.2°C and the annual precipitation is about 660 mm
 188 (Keyvanshokouhi et al., 2016). Both soils are neutral to slightly acidic and are characterized by
 189 the presence of a clay accumulation Bt horizon with clay content reaching 30 % for
 190 Feucherolles and 27 % for Mons, while the upper horizons are poorer in clay (17 % for
 191 Feucherolles and 20% for Mons).

192 The ^{14}C data from the soils of both sites were obtained after chemical treatment done at LSCE
 193 using a protocol adapted to achieve carbonate leaching without any loss of organic carbon, and
 194 ^{14}C activity measurement performed by AMS at the French LMC14 facility (Cottureau et al.,
 195 2007).

196 2.3.2 Congo site

197 The studied site is located in Kissoko (4.35°S, 11.75°E). It belongs to the SOERE F-ORE-T
 198 field observation sites of Pointe Noire, Congo Republic. The mean annual air temperature is of
 199 about 25°C with low seasonal variations ($\pm 5^\circ\text{C}$) and annual precipitation averages 1400mm
 200 with a dry season between June and September. The deep acidic sandy soil is a ferralic Arenosol



201 (WRB, 2006). The soil is characterized by a sand content larger than 90% (Laclau et al., 2000).
 202 Native vegetation is a savanna dominated by C4 plants (Epron et al., 2009) and the selected soil
 203 profile is under this native savanna vegetation. ^{14}C analyses were made in the same way as with
 204 the measurements for the two French sites, using the LSCE chemical treatment and the French
 205 LMC14 facility (Cottureau et al., 2007).

206 2.3.3 Argentina site

207 The Province of Misiones is located in northeastern Argentina. The climate is subtropical humid
 208 without a dry season, a 20°C of mean annual temperature and 1850mm of mean annual rainfall
 209 (Morrás et al., 2009). The profile used in this study is located in the southern part of Misiones
 210 (27°S , 55°W). Native vegetation is a forest dominated by C3 plants. The soil selected is an
 211 Acrisol (WRB, 2006). It's a red clay soil, strongly to very strongly acid with a clay content
 212 varying from 40% at the surface to 60% at 1m depth. ^{14}C measurements were made using a new
 213 Compact Radiocarbon System called *ECHoMICADAS* (Environment, Climate, Human, Mini
 214 Carbon Dating System) (Tisnérat-Laborde et al., 2015).

215 For the four sites, the SOC (kg m^{-3}), for each depth z , using the following equation was
 216 calculated using carbon content and bulk density data:

$$217 \text{SOC}_z = \text{OCC}_z * \text{BD}_z \quad (7)$$

218 Where OCC (wt %) is the carbon content and BD (kg m^{-3}) is the bulk density.

219 2.4 Different model tests

220 After the implementation of radiocarbon in the model, different tests were made (Table 2). Here
 221 we represent the outputs provided by three simulations:

- 222 i- Simulation using the initial version ORCHIDEE-SOM- ^{14}C (Model_Control in figures
 223 and tables) in which no changes were made. The diffusion has been kept constant
 224 throughout the profile ($D = 1.10^{-4} \text{ m}^2 \text{ year}^{-1}$) and the other parameters are those of the
 225 detailed version in Camino-Serrano et al., (2017).
- 226 ii- Simulation using the initial version ORCHIDEE-SOM- ^{14}C in which we modified some
 227 parameters following He et al. [2016] (Model_Test He in figures and tables). In brief,
 228 they used ^{14}C data from 157 globally distributed soil profiles sampled to 1-meter depth
 229 to evaluate CMIP5 models. Their results show that ESMs underestimated the mean age
 230 of soil carbon by a factor of more than six and overestimated the carbon sequestration
 231 potential of soils by a factor of nearly two. So, the suggestion (that we apply in this
 232 simulation) for the IPSL model was to multiply by 14 the turnover rate of the passive
 233 pool and by 0.07 the flux from slow pool to passive pool (Table 2). So, here, the
 234 diffusion was kept constant throughout the profile ($D = 1.10^{-4} \text{ m}^2 \text{ year}^{-1}$) but the turnover
 235 time of the passive pool increased from 462 years to 6468 years and the flux from the
 236 slow pool to the passive pool decreased from 0.07 to 0.049.
- 237 iii- Simulation using the initial version ORCHIDEE-SOM- ^{14}C in which we assume that the
 238 diffusion, initially constant throughout the profile, varies as a function of the depth
 239 (Model_Test Diffusion in figures and tables) according to the equation below:

$$240 D(z) = 5.42. 10^{-4} e^{(-0.04z)} \quad (8)$$



241 Where D is the diffusion ($\text{m}^2 \text{ year}^{-1}$) at a specific depth and z is the depth. This equation of
242 diffusion varying as a function of depth following Jagercikova et al. (2014) and assume that
243 bioturbation is higher in top soil than in deep soil.

244 2.5 Model simulations

245 First of all, in order to reach a steady state of the soil module, we ran the model over 12700
246 years (spinup). The state at the last time step of this spinup will then be used as initial state for
247 the simulations. For this, the CRUNCEP meteorological data for the period 1901-1910 were
248 used. This has been applied for Misiones, Feucherolles and Mons. However, for Kissoko, a first
249 spinup similar to the other sites was carried out but a second one (over approximately 4200
250 years) was also done after the end of the first to take into account the change of the land cover
251 from a tropical forest to a C4 savanna at this site (Schwartz et al., 1992). The atmospheric CO_2
252 concentration has been set at 296 ppm (year 1901, (Keeling and Whorf, 2006)) for the spinups.
253 For each site, specific pH, clay content and bulk density values were used (Table 1). It should
254 be noted that for these last data, only one value (the mean value on the profile) is provided as
255 input for the model

256 The simulations were then run at a yearly time step, from 1900 to 2011. A yearly atmospheric
257 CO_2 concentration value (Keeling and Whorf, 2006) is read for the sites. Of course, the same
258 specific pH, clay content and bulk density values were used (Table 1).

259 Figure 2 shows the evolution of the F^{14}C values in the atmosphere used in our model for
260 Argentina, Congo and France (Figure 5 from Hua et al. (2013)). In fact, the values provided are
261 classified into five zones, 3 in the Northern Hemisphere (NH) and 2 in the Southern Hemisphere
262 (SH), corresponding to different levels of ^{14}C . For France, the values correspond to the NH
263 zone 2, for the Congo to the SH zone 3 and finally for Argentina to the SH zone 1-2. Thus, for
264 our simulations, a yearly value is read for each site.

265 An F^{14}C value of 1.8 represents a doubling of the amount of ^{14}C in atmospheric CO_2 . On figure
266 2, it can be noted that the values recorded in France (northern hemisphere) are higher than those
267 in the Congo and Argentina (southern hemisphere). This is due to the preponderance of
268 atmospheric tests in the northern hemisphere and the time required to mix air across the equator.

269 2.6 Statistical analysis

270 Simulating carbon processes in soil requires comparison between the model outputs and the
271 measurements to test the model accuracy and possibly implement further improvement.
272 Statistical analysis based on the statistics of deviation were done to evaluate the model–
273 measurement discrepancy according to Kobayashi and Salam (2000) (where a detailed
274 description of the method is provided). Here, we only represent the different equations used. x
275 refers to the model outputs and y to the measurements.

$$276 \text{RMSD} = \sqrt{\frac{1}{n} \sum_{i=1}^n (x_i - y_i)^2} \quad (9)$$

277 RMSD is the Root Mean Squared Deviation, which represents the mean distance between
278 simulation and measurement.

$$279 \text{MSD} = \frac{1}{n} \sum_{i=1}^n (x_i - y_i)^2 = (\bar{x} - \bar{y})^2 + \frac{1}{n} \sum_{i=1}^n [(x_i - \bar{x}) - (y_i - \bar{y})]^2 \quad (10)$$



280 MSD, the Mean Squared Deviation, is the square of RMSD. The lower the value of MSD, the
281 closer the simulation is to the measurement.

$$282 \quad SB = (\bar{x} - \bar{y})^2 \quad (11)$$

283 Where \bar{x} and \bar{y} are the means of x_i (model outputs) and y_i (measurements) respectively.

284 SB is a part of the MSD (Eq.13) and represents the bias of the simulation from the measurement.

$$285 \quad SD_s = \sqrt{\frac{1}{n} \sum_{i=1}^n (x_i - \bar{x})^2} \quad (12)$$

286 SD_s is the Standard Deviation of the simulation.

$$287 \quad SD_m = \sqrt{\frac{1}{n} \sum_{i=1}^n (y_i - \bar{y})^2} \quad (13)$$

288 SD_m is the Standard Deviation of the measurements.

$$289 \quad r = \frac{\frac{1}{n} \sum_{i=1}^n (x_i - \bar{x})(y_i - \bar{y})}{SD_m SD_s} \quad (14)$$

290 Where r is the correlation coefficient between the simulation and measurements.

$$291 \quad SDSD = (SD_s - SD_m)^2 \quad (15)$$

292 SDSD here, is the difference in the magnitude of fluctuation between the simulation and
293 measurements.

$$294 \quad LCS = 2SD_s SD_m(1 - r) \quad (16)$$

295 LSC represents the lack of positive correlation weighted by the standard deviations.

296 Finally, with all the above terms combined, the MSD can be written as:

$$297 \quad MSD = SB + SDSD + LCS \quad (17)$$

298 For the different simulations, the MSD and its components were calculated according to the
299 total soil carbon and to the $F^{14}C$.

300

301 **3 Model results and evaluation**

302 **3.1 Outputs from simulation using the initial version of the model ORCHIDEE-SOM- ^{14}C** 303 **(Model_Control)**

304 **3.1.1 Simulated total soil carbon**

305 Results from the initial version of ORCHIDEE-SOM- ^{14}C show that in all the studied sites, the
306 model succeeds in reproducing the trend of the total carbon profiles, with more carbon at the
307 surface which decreases then according to the depth (Figure 3). Moreover, total soil carbon
308 stock simulated down to 2m depth is in accordance with data in the case of Misiones and
309 Feucherolles where the major difference mainly lies on the surface. This results in correlation
310 coefficients of 0.55 and 0.6 respectively (Table 3). For the sites of Kissoko and Mons, an over-
311 estimation of the total soil carbon is marked to 50cm deep for Kissoko (then it decreases) and
312 up to 120cm deep for Mons. Correlation coefficients are 0.4 and 0.75 for Kissoko and Mons
313 respectively (Table 3).



314 Metrics presented in Figure 4, showed that this version (ORCHIDEE-SOM- ^{14}C) represents
315 relatively well the observation from Feucherolles ($\text{MSD} = 206 \text{ kg C m}^{-3}$), whereas the other are
316 highly overestimated (Kissoko, $\text{MSD} = 1343 \text{ kg C m}^{-3}$; Misiones $\text{MSD} = 2180 \text{ kg C m}^{-3}$; Mons
317 $\text{MSD} = 3355 \text{ kg C m}^{-3}$). Then, by detailing the different components of the MSD (Figure 4), we
318 note that for Mons and Kissoko, standard bias (SB) is the major component of the MSD with
319 70% and 60% respectively. This reflects that the average of total soil carbon over the soil profile
320 simulated by the model is primarily the origin of the deviation of the model outputs from data.
321 The mean total soil carbon estimated by the model (Table 3) is more than four times the mean
322 total carbon measured for Mons (64 kg C m^{-3} against 15 kg C m^{-3} respectively) and it is more
323 than eight times that measured for Kissoko (34 kg C m^{-3} against 4 kg C m^{-3} respectively). This
324 significant gap recorded in the case of the Kissoko site, where the measured SOC is very low,
325 is probably due to its very particular soil characteristics (acidic sandy soil). ORCHIDEE is a
326 global model that is not parameterized for such specific soil conditions

327 However, the main components of MSD for Feucherolles and Misiones are both SB (46% and
328 56% for Feucherolles and Misiones, respectively) and also LCS (53 and 31% for Feucherolles
329 and Misiones, respectively). This means that for these two sites, the deviation between model
330 outputs and measurements is mainly due to a variation of carbon stock estimation throughout
331 the profile. The mean total soil carbon estimated in these both cases (Table 3) is only 1.7 to 2
332 times higher than those measured (65 kg C m^{-3} estimated against 31 kg C m^{-3} measured for
333 Misiones and 24 kg C m^{-3} estimated against 14 kg C m^{-3} measured for Feucherolles).

334 The vertical profile of the SOC stock simulated was thereby globally not very far from that of
335 the data. The overestimation, especially at the top, suggests that the distribution of the litter
336 following the root profile and / or the vertical transport of SOC by diffusion are not correctly
337 described in the model

338 3.1.2 Simulated F^{14}C

339 Regarding the ^{14}C activity, bulk F^{14}C profiles show classical pattern with higher ^{14}C activity,
340 on the top, slightly influenced by the peak bomb more enriched years. Subsequently profiles
341 show decreasing ^{14}C activity with depth (Figure 5).

342 The estimated profiles (Model-Control) follow the same trend with a decrease from the surface
343 to the depth. However, there is a significant difference between the estimated values and those
344 measured throughout the profile. The statistical analyzes (Figure 6) provide MSD values: 0.02
345 for Mons and Misiones, 0.03 for Kissoko and 0.09 for Feucherolles. The major component of
346 the MSD in the four sites is the LCS, with a proportion always greater than 50% and which is
347 even 90% for Mons, 80% for Misiones and 70% for Congo, however, it is only 55% for
348 Feucherolles. The high proportions of LCS suggest that the model fails to reproduce the shape
349 of the profile. The lower values estimated by the models reflect a more modern carbon age than
350 in reality. This can be explained, first, by the fact that the root profile puts too much fresh
351 organic carbon in deep soil. Afterwards, in ORCHIDEE, root profile is assumed to follow an
352 exponential without modulation due to environmental conditions.

353 Then, SB's contribution does not exceed 7% for Misiones, Kissoko and Mons but reaches about
354 40% for Feucherolles. This reflects that the mean value of the F^{14}C estimated by the model and



355 that obtained after the measurements are not very different, except for Feucherolles site (Table
356 4). Indeed, the average value estimated for Misiones is 0.920, very close to that measured at
357 0.930, 0.995 for Kissoko against 0.985 measured and 0.860 for Mons against 0.815 measured.
358 Yet, the difference is greater for the Feucherolles site, the estimated value being 0.915 while
359 the measurement is 0.725. This difference might be caused by the low $F^{14}C$ value measured at
360 150cm (0.257), that the model is not able to capture. This suggests that modeled deep soil
361 carbon is much younger than the observed total soil carbon, probably because ORCHIDEE-
362 SOM simulates a relatively small proportion of passive pool in the lower soil horizons (Figure
363 7), while an increasing proportion of passive carbon with soil depth could be expected.

364 In brief, SOC stocks are generally overestimated and soil carbon age in deep soils (as shown
365 by the $F^{14}C$) is underestimated, suggesting that the turnover rate of passive pool is subject to
366 improvements in ORCHIDEE-SOM.

367 **3.2 Outputs from simulation using the initial version of the model ORCHIDEE-SOM- ^{14}C** 368 **including He's suggestion (Model_Test He)**

369 **3.2.1 Simulated total soil carbon**

370 Figure 3 shows profiles output after He's suggestion implemented into ORCHIDEE-SOM- ^{14}C
371 (green dotted curves). Resulting profiles follow the same trend than observations but in this
372 case (Model_Test He), the overestimation is very high from the surface to the depth. This is
373 further confirmed by the metrics analysis (Figure 4). MSD values markedly increased, resulting
374 in an even higher variance. Obviously, the major component of MSD in all cases is the SB
375 (varying from 80% to 87%) reflecting an even more marked overestimation of the mean total
376 carbon estimates: 128 kg C m $^{-3}$ against 31 kg C m $^{-3}$ for Misiones, 53 kg C m $^{-3}$ against 4 kg C
377 m $^{-3}$ for Kissoko, 24 kg C m $^{-3}$ against 14 kg C m $^{-3}$ for Feucherolles and 131 kg C m $^{-3}$ against 15
378 kg C m $^{-3}$ for Mons.

379 **3.2.2 Simulated $F^{14}C$**

380 Model_Test He outputs (Figure 5, green dotted curves) for $F^{14}C$ are once again even further
381 away from observations and MSDs (Figure 6) are much higher, except for Feucherolles, which
382 MSD value in this case is lower. The MSD components for Feucherolles site show that the LCS
383 increases from 0.05 to 0.06 whereas it is the SB which decreased from 0.04 to 0.03, again
384 reflecting a variation of the profile more than a difference from the means.

385 Improvement of the model-measurement fit for the $F^{14}C$ at 150 cm in Feucherolles confirms
386 that the deep soil carbon simulated by the control version of ORCHIDEE-SOM- ^{14}C was
387 excessively young, since the longer residence time of the passive pool reported by He et al.
388 (2016) resulted in a higher proportion of passive pool across the soil profile (Figure 7), thus
389 improving deep soil carbon age. Nevertheless, this test only improves the simulation of deep
390 soil carbon in Feucherolles. On the contrary, this increase in carbon residence time has even
391 more deviated the outputs of the model for all the other cases (Figure 5 and 6).

392 Indeed, taking the priming effect into account in this new version of ORCHIDEE has
393 contributed to a 50% of decrease in carbon storage over the historical period. He's correction
394 was also aimed at reducing this storage and is then of the same order of magnitude as the
395 priming effect. Thus, applying He's correction to this version of the model, which takes into



396 account the priming effect, contributes to a double correction for the same target, which then
397 generates this important difference between model outputs and measurements. Moreover, the
398 work of He et al. (2016) is done under the standard parameterization of ORCHIDEE based on
399 Century, while ORCHIDEE-SOM was re-parameterized after adding several different
400 processes, the priming effect among them (Camino-Serrano et al., 2017), what makes it difficult
401 to associate results from her and this study.

402 **3.3 Outputs from simulation using the initial version of the model ORCHIDEE-SOM-¹⁴C** 403 **with diffusion varying according to the depth (Model_Test Diffusion)**

404 **3.3.1 Simulated total soil carbon**

405 Fick's law of diffusion is classically used in models to represent bioturbation (Elzein and
406 Balesdent, 1995; Guenet et al., 2013; Koven et al., 2013; O'Brien and Stout, 1978; Wynn et al.,
407 2005). Using a fixed diffusion constant implicitly suggests that soil fauna activity is uniform
408 over the entire soil profile. This is fact generally the case of several models of diffusion
409 especially used at the level of an ecosystem (Bruun et al., 2007; Guimberteau et al., 2017;
410 O'Brien and Stout, 1978). However soil faunal activity vary naturally with depth, in addition,
411 the characteristics of a soil, i.e. its structure and pore distribution, may vary depending on the
412 depth, so, the diffusion coefficient should be depth-dependent (Jagercikova et al., 2014).

413 With Model_Test Diffusion, the carbon profiles (orange dashed curves) was improved
414 compared to the initial outputs (Model_Control). The overestimation at the surface decreases
415 at the four sites (Figure 3). In particular, the Misiones outputs fit very well the observed profiles.
416 This is confirmed with lower MSDs for the four sites for this version compared to
417 Model_Control showing a much smaller deviation from the measurements (Figure 4).

418 Anyway, the total SOC stocks simulated according to this third simulation are closer to the
419 measured values and describing the vertical transport of SOC through diffusion varying
420 according to the depth improves significantly the model outputs.

421 **3.3.2 Simulated F¹⁴C**

422 Regarding the F¹⁴C outputs, the simulations using the initial version ORCHIDEE-SOM-¹⁴C in
423 which we assume that the diffusion varies as a function of the depth (Model_Test Diffusion)
424 results in an improvement of the F¹⁴C profiles (orange dashes curves) especially for the sites
425 Misiones, Mons and Kissoko (Figure 5). Statistical analyzes prove it with significantly lower
426 MSDs. In addition, the proportion of LCS is 98%, 92% and 88% for Mons, Misiones and
427 Kissoko, respectively, highlighting an estimated average very close to the measurements with
428 a clear disparity, less marked than with the first two simulations, throughout the profile (Figure
429 6). Overall, the simulated F¹⁴C to 2 m of depth according to this third simulation are in a better
430 agreement with the measured values, thus, diffusion varying according to the depth improves
431 significantly the model outputs.

432 Using a diffusion coefficient that varies as a function of the depth, seems to correct the
433 overestimation of the surface total soil carbon by increasing the proportion of labile soil carbon
434 pools in the first soil layers.



435 When we look at the relative proportion of each of the soil carbon pools summing the total soil
436 carbon at each soil layer (Figure 7), we note that it is mainly the distribution of the litter
437 according to the depth which varied. In fact, the structural litter proportion is multiplied by
438 about 2 in all four cases, and this proportion remains as large at the surface as at depth. This
439 increase in litter proportion has also resulted in a decrease in the passive pool, more pronounced
440 at the surface but also important at depth (except for Feucherolles where the decrease is only
441 marked at the bottom). It suggests that the vertical carbon distribution, which is largely modified
442 by the diffusion coefficient, greatly impacts the SOC and ^{14}C profiles, which is in line with
443 Dwivedi et al. (2017) who found that the vertical carbon input profiles were important controls
444 over the ^{14}C depth distribution.

445 In this study, the vertical transport of SOC and litter through diffusion has been improved by
446 varying diffusion according to the depth. Further model development should explore the impact
447 of the other process defining the soil carbon pools vertical distribution especially the
448 distribution of the litter according to the root profile.

449 Overall, by using radiocarbon (^{14}C) measurements we have been able to diagnose internal
450 model biases (underestimation of deep soil carbon age) and to propose further model
451 improvements (depth-dependent diffusion). Therefore, the use of radiocarbon (^{14}C) tracers in
452 global models emerges as a promising tool to constraint not only SOC turnover times in the
453 long-term (He et al., 2016), but also internal SOC processes and fluxes that are has no direct
454 comparison with field measurements.

455

456 **4 conclusion**

457 ORCHIDEE-SOM- ^{14}C , is one of the first land surface models that incorporates the ^{14}C dynamic
458 in the soil. Its starting point is ORCHIDEE-SOM, a recently developed soil model. We
459 evaluated the new model ORCHIDEE-SOM- ^{14}C for four sites in different biomes. The model
460 almost managed to reproduce the soil organic carbon stocks and the ^{14}C content along the
461 vertical profiles at the four sites. However, an overestimation of the total carbon stock
462 throughout the profile was noted, but was mostly marked on the surface. Then, by using
463 radiocarbon (^{14}C) measurements, we have been able to diagnose internal model biases
464 (underestimation of deep soil carbon age) and to propose further model improvements (depth-
465 dependent diffusion). The importance of diffusion has also been highlighted as by making it
466 varies according to the depth, the model outputs have been improved. This suggests that, from
467 now on, model improvements should mainly focus on a depth dependent parameterization,
468 mainly for the diffusion. The next step will deal with the comparison of model outputs to data
469 at larger scales to be able to run the new version ORCHIDEE-SOM- ^{14}C at both regional and
470 global scales.

471

472

473

474



475 **Code availability**

476 The version of the code is freely available here:

477 <https://forge.ipsl.jussieu.fr/orchidee/wiki/GroupActivities/CodeAvailabilityPublication/ORC>
478 [HIDEE_gmd-2018-14C](#)

479

480 **Acknowledgement**

481 This study, part of the MT's PhD, financed by the University of Versailles Saint Quentin, is
482 within the scope of the ANR-14-CE01-0004 DeDyCAS project. Marta Camino-Serrano
483 acknowledges funding from the European Research Council Synergy grant ERC- 2013-SyG-
484 610028 IMBALANCE-P. Part of the data were acquired in the frame of the AGRIPED project
485 (ANR 2010 BLAN 605).

486

487 **References**

- 488 Balesdent, J. and Guillet, B.: Les datations par le ¹⁴C des matières organiques des sols.
489 Contribution à l'étude de l'humification et du renouvellement des substances
490 humiqueétriques, *Sci. du sol*, 2, 93–111, 1982.
- 491 Braakhekke, M. C., Beer, C., Hoosbeek, M. R., Reichstein, M., Kruijt, B., Schruppf, M. and
492 Kabat, P.: Somprof: A vertically explicit soil organic matter model, *Ecol. Modell.*, 222(10),
493 1712–1730, doi:10.1016/j.ecolmodel.2011.02.015, 2011.
- 494 Bruun, S., Christensen, B. T., Thomsen, I. K., Jensen, E. S. and Jensen, L. S.: Modeling
495 vertical movement of organic matter in a soil incubated for 41 years with ¹⁴C labeled straw,
496 *Soil Biol. Biochem.*, 39(1), 368–371, doi:10.1016/j.soilbio.2006.07.003, 2007.
- 497 Camino-Serrano, M., Guenet, B., Luysaert, S., Ciais, P., Bastrikov, V., De Vos, B., Gielen,
498 B., Gleixner, G., Jornet-Puig, A., Kaiser, K., Kothawala, D., Lauerwald, R., Peñuelas, J.,
499 Schruppf, M., Vicca, S., Vuichard, N., Walmsley, D. and Janssens, I. A.: ORCHIDEE-SOM:
500 Modeling soil organic carbon (SOC) and dissolved organic carbon (DOC) dynamics along
501 vertical soil profiles in Europe, *Geosci. Model Dev. Discuss.*, 1–38, doi:10.5194/gmd-2017-
502 255, 2017.
- 503 Coleman, K., Jenkinson, D. S., Crocker, G. J., Grace, P. R., Klír, J., Körschens, M., Poulton,
504 P. R. and Richter, D. D.: Simulating trends in soil organic carbon in long-term experiments
505 using RothC-26.3, *Geoderma*, 81(1–2), 29–44, doi:10.1016/S0016-7061(97)00079-7, 1997.
- 506 Cottreau, E., Arnold, M., Moreau, C., Baqué, D., Bavay, D., Caffy, I., Comby, C.,
507 Dumoulin, J.-P., Hain, S., Perron, M., Salomon, J. and Setti, V.: Artemis, the New ¹⁴C AMS
508 at LMC14 in Saclay, France, *Radiocarbon*, 49(2), 291–299, doi:10.2458/azu_js_rc.49.2928,
509 2007.
- 510 Delibrias, G., Guillier, M. T. and Labeyrie, J.: Saclay natural radiocarbon measurements i,
511 *Radiocarbon*, 6, 233–250 [online] Available from:
512 <http://radiocarbon.library.arizona.edu/radiocarbon/GetFileServlet?file=file:///data1/pdf/Radio>
513 [carbon/Volume6/Number1/azu_radiocarbon_v6_233_250_v.pdf&type=application/pdf](http://radiocarbon.library.arizona.edu/radiocarbon/GetFileServlet?file=file:///data1/pdf/Radio), 1964.
- 514 Ducoudré, N. I., Laval, K. and Perrier, A.: SECHIBA, a New Set of Parameterizations of the
515 Hydrologic Exchanges at the Land-Atmosphere Interface within the LMD Atmospheric
516 General Circulation Model, *J. Clim.*, 6, 248–273, doi:10.1175/1520-



- 517 0442(1993)006<0248:SANSOP>2.0.CO;2, 1993.
- 518 Dwivedi, D., Riley, W. J., Torn, M. S., Spycher, N., Maggi, F. and Tang, J. Y.: Mineral
519 properties, microbes, transport, and plant-input profiles control vertical distribution and age of
520 soil carbon stocks, *Soil Biol. Biochem.*, 107, 244–259, doi:10.1016/j.soilbio.2016.12.019,
521 2017.
- 522 Elliott, E. T., Paustian, K. and Frey, S. D.: Modeling the Measurable or Measuring the
523 Modelable: A Hierarchical Approach to Isolating Meaningful Soil Organic Matter
524 Fractionations, in *Evaluation of Soil Organic Matter Models*, pp. 161–179, Springer Berlin
525 Heidelberg, Berlin, Heidelberg., 1996.
- 526 Elzein, A. and Balesdent, J.: Mechanistic simulation of vertical distribution of carbon
527 concentrations and residence times in soils, *Soil Sci. Soc. Am. J.*, 59(5), 1328–1335,
528 doi:10.1017/CBO9781107415324.004, 1995.
- 529 Epron, D., Marsden, C., M'Bou, A. T., Saint-André, L., d'Annunzio, R. and Nouvellon, Y.:
530 Soil carbon dynamics following afforestation of a tropical savannah with Eucalyptus in
531 Congo, *Plant Soil*, 323(1), 309–322, doi:10.1007/s11104-009-9939-7, 2009.
- 532 Godwin, H.: Half-life of radiocarbon, *Nature*, 195(4845), 984, doi:10.1038/195984a0, 1962.
- 533 Guenet, B., Eglin, T., Vasilyeva, N., Peylin, P., Ciais, P. and Chenu, C.: The relative
534 importance of decomposition and transport mechanisms in accounting for soil organic carbon
535 profiles, *Biogeosciences*, 10(4), 2379–2392, doi:10.5194/bg-10-2379-2013, 2013.
- 536 Guenet, B., Moyano, F. E., Peylin, P., Ciais, P. and Janssens, I. A.: Towards a representation
537 of priming on soil carbon decomposition in the global land biosphere model ORCHIDEE
538 (version 1.9.5.2), *Geosci. Model Dev*, 9, 841–855, doi:10.5194/gmd-9-841-2016, 2016.
- 539 Guimberteau, M., Zhu, D., Maignan, F., Huang, Y., Yue, C., Dantec-Nédélec, S., Ottlé, C.,
540 Jorner-Puig, A., Bastos, A., Laurent, P., Goll, D., Bowring, S., Chang, J., Guenet, B., Tifafi,
541 M., Peng, S., Krinner, G., Ducharne, A., Wang, F., Wang, T., Wang, X., Wang, Y., Yin, Z.,
542 Lauerwald, R., Joetzjer, E., Qiu, C., Kim, H. and Ciais, P.: ORCHIDEE-MICT (revision
543 4126), a land surface model for the high-latitudes: model description and validation, *Geosci.*
544 *Model Dev. Discuss.*, 1–65, doi:10.5194/gmd-2017-122, 2017.
- 545 He, Y., Trumbore, S. E., Torn, M. S., Harden, J. W., Vaughn, L. J. S., Allison, S. D. and
546 Randerson, J. T.: Radiocarbon constraints imply reduced carbon uptake by soils during the
547 21st century, *Science* (80-.), 353(6306) [online] Available from:
548 <http://science.sciencemag.org/content/353/6306/1419.full> (Accessed 10 October 2017), 2016.
- 549 Hua, Q., Barbetti, M. and Rakowski, A. Z.: Atmospheric Radiocarbon for the Period 1950–
550 2010, *Radiocarbon*, 55(4), 2059–2072, doi:10.2458/azu_js_rc.v55i2.16177, 2013.
- 551 Jagercikova, M., Evrard, O., Balesdent, J., Lefèvre, I. and Cornu, S.: Modeling the migration
552 of fallout radionuclides to quantify the contemporary transfer of fine particles in Luvisol
553 profiles under different land uses and farming practices, *Soil Tillage Res.*, 140, 82–97,
554 doi:10.1016/j.still.2014.02.013, 2014.
- 555 Jastrow, J. D., Amonette, J. E. and Bailey, V. L.: Mechanisms controlling soil carbon turnover
556 and their potential application for enhancing carbon sequestration, *Clim. Change*, 80, 5–23,
557 doi:10.1007/s10584-006-9178-3, 2007.
- 558 Kalnay, E., Kanamitsu, M., Kistler, R., Collins, W., Deaven, D., Gandin, L., Iredell, M., Saha,
559 S., White, G., Woollen, J., Zhu, Y., Leetmaa, A., Reynolds, R., Chelliah, M., Ebisuzaki, W.,
560 Higgins, W., Janowiak, J., Mo, K. C., Ropelewski, C., Wang, J., Jenne, R., Joseph, D.,
561 Kalnay, E., Kanamitsu, M., Kistler, R., Collins, W., Deaven, D., Gandin, L., Iredell, M., Saha,



- 562 S., White, G., Woollen, J., Zhu, Y., Leetmaa, A., Reynolds, R., Chelliah, M., Ebisuzaki, W.,
563 Higgins, W., Janowiak, J., Mo, K. C., Ropelewski, C., Wang, J., Jenne, R. and Joseph, D.:
564 The NCEP/NCAR 40-Year Reanalysis Project, *Bull. Am. Meteorol. Soc.*, 77(3), 437–471,
565 doi:10.1175/1520-0477(1996)077<0437:TNYRP>2.0.CO;2, 1996.
- 566 Keeling, C. D. and Whorf, T. P.: Atmospheric CO₂ records from sites in the SIO air sampling
567 network., in *Oak Ridge National Laboratory U.S. Department of Energy, Oak Ridge, Tenn*
568 *U.S.*, 2006.
- 569 Keyvanshokouhi, S., Cornu, S., Samouëlian, A. and Finke, P.: Evaluating SoilGen2 as a tool
570 for projecting soil evolution induced by global change, *Sci. Total Environ.*, 571, 110–123,
571 doi:10.1016/j.scitotenv.2016.07.119, 2016.
- 572 Kobayashi, K. and Salam, M. U.: Comparing simulated and measured values using mean
573 squared deviation and its components, *Agron. J.*, 92(2), 345–352,
574 doi:10.2134/agronj2000.922345x, 2000.
- 575 Koven, C. D., Riley, W. J., Subin, Z. M., Tang, J. Y., Torn, M. S., Collins, W. D., Bonan, G.
576 B., Lawrence, D. M. and Swenson, S. C.: The effect of vertically resolved soil
577 biogeochemistry and alternate soil C and N models on C dynamics of CLM4, *Biogeosciences*,
578 10(11), 7109–7131, doi:10.5194/bg-10-7109-2013, 2013.
- 579 Krinner, G., Viovy, N., de Noblet-Ducoudré, N., Ogée, J., Polcher, J., Friedlingstein, P.,
580 Ciais, P., Sitch, S. and Prentice, I. C.: A dynamic global vegetation model for studies of the
581 coupled atmosphere-biosphere system, *Global Biogeochem. Cycles*, 19(1),
582 doi:10.1029/2003GB002199, 2005.
- 583 Laclau, J. P., Bouillet, J. P. and Ranger, J.: Dynamics of biomass and nutrient accumulation in
584 a clonal plantation of Eucalyptus in Congo, *For. Ecol. Manage.*, 128(3), 181–196,
585 doi:10.1016/S0378-1127(99)00146-2, 2000.
- 586 Mitchell, T. D., Carter, T. R., Jones, P. D., Hulme, M. and New, M. A.: A comprehensive set
587 of high-resolution grids of monthly climate for Europe and the globe: the observed record
588 (1901–2000) and 16 scenarios (2001–2100), *Tyndall Cent. Clim. Chang. Res.*, 1–30 [online]
589 Available from: http://www.ipcc-data.org/docs/tyndall_working_papers_wp55.pdf, 2004.
- 590 Morrás, H., Moretti, L., Píccolo, G. and Zech, W.: Genesis of subtropical soils with stony
591 horizons in NE Argentina: Autochthony and polygenesis, *Quat. Int.*, 196(1), 137–159,
592 doi:10.1016/j.quaint.2008.07.001, 2009.
- 593 O’Brien, B. J. and Stout, J. D.: Movement and turnover of soil organic matter as indicated by
594 carbon isotope measurements, *Soil Biol. Biochem.*, 10(4), 309–317, doi:10.1016/0038-
595 0717(78)90028-7, 1978.
- 596 Parton, W. J., Schimel, D. S., Cole, C. V. and Ojima, D. S.: Analysis of factors controlling
597 soil organic matter levels in great plains grasslands, *Soil Sci. Soc. Am. J.*, 51(5), 1173–1179,
598 doi:10.2136/sssaj1987.03615995005100050015x, 1987.
- 599 Parton, W. J., Stewart, J. W. B. and Cole, C. V.: Dynamics of C, N, P and S in grassland soils:
600 a model, *Biogeochemistry*, 5(1), 109–131, doi:10.1007/BF02180320, 1988.
- 601 Reimer, P. J., Brown, T. A. and Reimer, R. W.: Discussion: reporting and calibration of post-
602 bomb 14C data., *Radiocarbon*, 46(1), 1299–1304, doi:10.2458/azu_js_rc.46.4183, 2004.
- 603 de Rosnay, P. and Polcher, J.: Modelling root water uptake in a complex land surface scheme
604 coupled to a GCM, *Hydrol. Earth Syst. Sci.*, 2(2/3), 239–255, doi:10.5194/hess-2-239-1998,
605 1998.



- 606 Scharpenseel, H. W. and Schiffmann, H.: Radiocarbon dating of soils, a review, *Zeitschrift*
607 *für Pflanzenernährung und Bodenkd.*, 140(2), 159–174, doi:10.1002/jpln.19771400205, 1977.
- 608 Schwartz, D., Mariotti, A., Trouve, C., Van Den Borg, K. and Guillet, B.: Etude des profils
609 isotopiques ^{13}C et ^{14}C d'un sol ferrallitique sableux du littoral congolais : implications sur la
610 dynamique de la matière organique et l'histoire de la végétation, *Comptes Rendus l'Académie*
611 *des Sci. 2 Mécanique...*, 1992, 315, p. 1411-1417. ISSN 0249-6305, 315, 1411–1417 [online]
612 Available from: <http://www.documentation.ird.fr/hor/fdi:37558> (Accessed 18 December
613 2017), 1992.
- 614 Sitch, S., Smith, B., Prentice, I. C., Arneth, a., Bondeau, a., Cramer, W., Kaplan, J. O.,
615 Levis, S., Lucht, W., Sykes, M. T., Thonicke, K. and Venevsky, S.: Evaluation of ecosystem
616 dynamics, plant geography and terrestrial carbon cycling in the LPJ dynamic global
617 vegetation model, *Glob. Chang. Biol.*, 9(2), 161–185, doi:10.1046/j.1365-
618 2486.2003.00569.x, 2003.
- 619 Stuiver, M. and Polach, H. A.: Reporting of ^{14}C data, *Radiocarbon*, 19(3), 355–363,
620 doi:10.1016/j.forsciint.2010.11.013, 1977.
- 621 Taylor, K. E., Stouffer, R. J. and Meehl, G. A.: An overview of CMIP5 and the experiment
622 design, *Bull. Am. Meteorol. Soc.*, 93(4), 485–498, doi:10.1175/BAMS-D-11-00094.1, 2012.
- 623 Tisnérat-Laborde, N., Thil, F., Synal, H.-A., Hatté, C., Cersoy, S., Gauthier, C., Kaltnecker,
624 E., Massault, M., Michelot, J.-L., Noret, A., Noury, C., Siani, G., Tombret, O., Vigne, J.-D.,
625 Wacker, L. and Zazzo, A.: A new compact AMS facility measuring ^{14}C dedicated to
626 Environment, Climate and Human Sciences, in 22nd International Radiocarbon Conference,
627 Dakar, Senegal. November 2015. Oral presentation, pp. 16–20., 2015.
- 628 Todd-Brown, K. E. O., Randerson, J. T., Post, W. M., Hoffman, F. M., Tarnocai, C., Schuur,
629 E. A. G. and Allison, S. D.: Causes of variation in soil carbon simulations from CMIP5 Earth
630 system models and comparison with observations, *Biogeosciences*, 10(3), 1717–1736,
631 doi:10.5194/bg-10-1717-2013, 2013.
- 632 Trumbore, S.: Age of soil organic matter and soil respiration: Radiocarbon constraints on
633 belowground C dynamics, *Ecol. Appl.*, 10(2), 399–411, doi:10.1890/1051-
634 0761(2000)010[0399:AOSOMA]2.0.CO;2, 2000.
- 635 Wieder, W. R., Bonan, G. B. and Allison, S. D.: Global soil carbon projections are improved
636 by modelling microbial processes, *Nat. Clim. Chang.*, 3(10), 909–912,
637 doi:10.1038/nclimate1951, 2013.
- 638 WRB: World reference base for soil resources 2006: a framework for international
639 classification, correlation and communication., 2006.
- 640 Wynn, J. G., Bird, M. I. and Wong, V. N. L.: Rayleigh distillation and the depth profile of
641 $^{13}\text{C}/^{12}\text{C}$ ratios of soil organic carbon from soils of disparate texture in Iron Range National
642 Park, Far North Queensland, Australia, *Geochim. Cosmochim. Acta*, 69(8), 1961–1973,
643 doi:10.1016/j.gca.2004.09.003, 2005.
- 644
- 645
- 646
- 647
- 648



649 **Table 1.** General description of the studied sites. The mean bulk density, pH and clay fraction
650 values over the profiles were used as input for each site. For Mons and Feucherolles sites, min
651 and max values of pH and clay fraction are provided between brackets.

Site name	Feucherolles	Mons	Kissoko	Misiones
Sampling Date	April 2011	March 2011	May 2014	May 2015
Location	France	France	Congo	Argentina
Coordinates	48.90°N, 1.97°E	49.87°N, 3.03°E	4.35°S, 11.75°E	27.65°S, 55.42°W
Elevation (m)	120	88	100	NA
Mean Annual Rainfall (mm)	660	680	1400	1850
Mean Annual Temperature (°C)	11.2	11	25	20
Soil Type (WRB)	Luvisol	Luvisol	Arenosol	Acrisol
Land Use	Temperate broad-leaved summergreen forest	Grassland	Native savanna	Tropical broad-leaved evergreen forest
Mean Bulk Density (g cm⁻³)	1.34	1.4	1.48	1.15
Mean pH	5.9 (5.12-8.55)	6.9 (6.70-7.56)	5.2	5.2
Mean Clay Fraction (%)	20 % (13-30 %)	23 % (19-27 %)	5 %	58 %

652

653

654 **Table 2.** The main differences between the three simulations

	Flux from slow pool to passive pool	Turnover time of the passive pool (year)	Diffusion (m ² year ⁻¹)
Model_Control	0.07	462	$D(z) = 1.10^{-4}$
Model_Test He	0.049	6468	$D(z) = 1.10^{-4}$
Model_Test Diffusion	0.07	462	$D(z) = 5.42. 10^{-4} e^{(-0.04z)}$

655

656

657

658



659 **Table 3.** The correlation coefficient (r) between model outputs and measurements and the mean
 660 values (provided by the model and the measurements) over the profile according to total soil
 661 carbon (kg C m^{-3}), for the four sites. The results of the initial version of the model ORCHIDEE-
 662 SOM- ^{14}C (Model_Control) as well as those from the version including the modification if the
 663 passive pool turnover rate and the slow-to-passive flux revised according to (He et al., 2016)
 664 (Model_Test He) and diffusion varying according to the depth (Model_Test Diffusion), are
 665 provided.
 666

		r	Mean total soil carbon (kg C m^{-3}) Model	Mean total soil carbon (kg C m^{-3}) Measurements
Misiones	Model_Control	0.55	65	31±0.30
	Model_Test He	0.50	128	
	Model_Test Diffusion	0.60	57	
Kissoko	Model_Control	0.40	34	4±0.30
	Model_Test He	0.40	53	
	Model_Test Diffusion	0.50	31	
Feucherolles	Model_Control	0.60	24	14±0.08
	Model_Test He	0.60	42	
	Model_Test Diffusion	0.70	21	
Mons	Model_Control	0.75	64	15±0.10
	Model_Test He	0.70	131	
	Model_Test Diffusion	0.80	54	

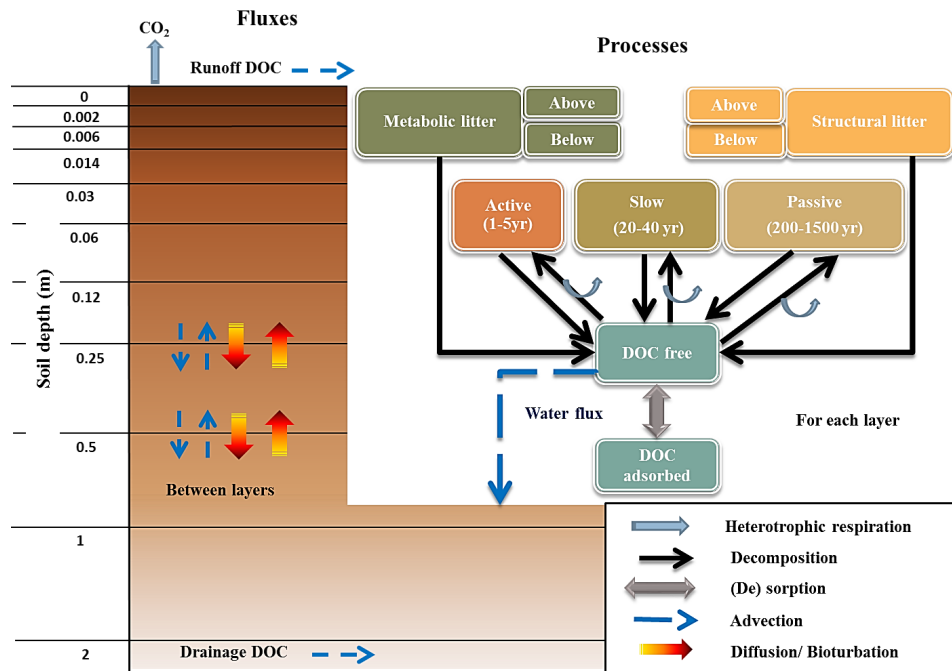
667

668 **Table 4.** The correlation coefficient (r) between model outputs and measurements and the mean
 669 values (provided by the model and the measurements) over the profile according to F^{14}C , for
 670 the four sites. The results of the initial version of the model ORCHIDEE-SOM- ^{14}C
 671 (Model_Control) as well as those from the version including the modification if the passive
 672 pool turnover rate and the slow-to-passive flux revised according to (He et al., 2016)
 673 (Model_Test He) and diffusion varying according to the depth (Model_Test Diffusion), are
 674 provided.
 675

675

		r	Mean Model	Mean Measurements
Misiones	Model_Control	0.55	0.920	0.930±0.009
	Model_Test He	0.50	0.560	
	Model_Test Diffusion	0.60	0.900	
Kissoko	Model_Control	0.40	0.995	0.985±0.004
	Model_Test He	0.30	0.620	
	Model_Test Diffusion	0.55	0.995	
Feucherolles	Model_Control	0.55	0.915	0.725±0.005
	Model_Test He	0.55	0.550	
	Model_Test Diffusion	0.60	0.890	
Mons	Model_Control	0.75	0.860	0.815±0.005
	Model_Test He	0.70	0.510	
	Model_Test Diffusion	0.80	0.835	

676

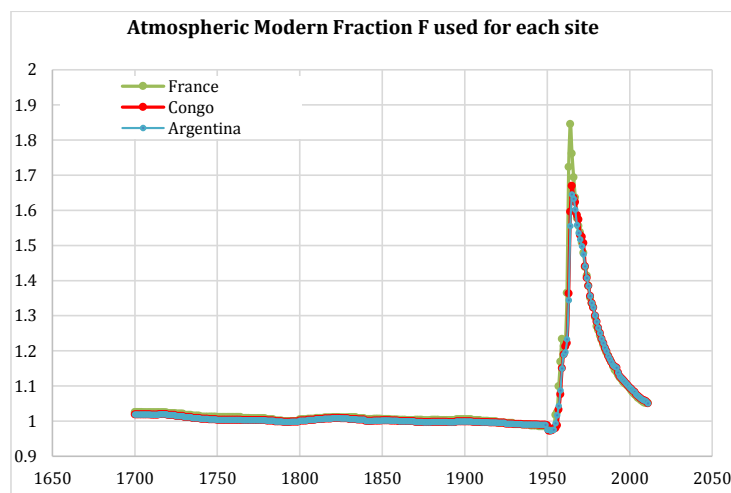


677

678

679 **Figure 1.** Overview of the different fluxes and processes in soil as presented in the version of
 680 ORCHIDEE-SOM adapted from Camino-Serrano et al. (2017)

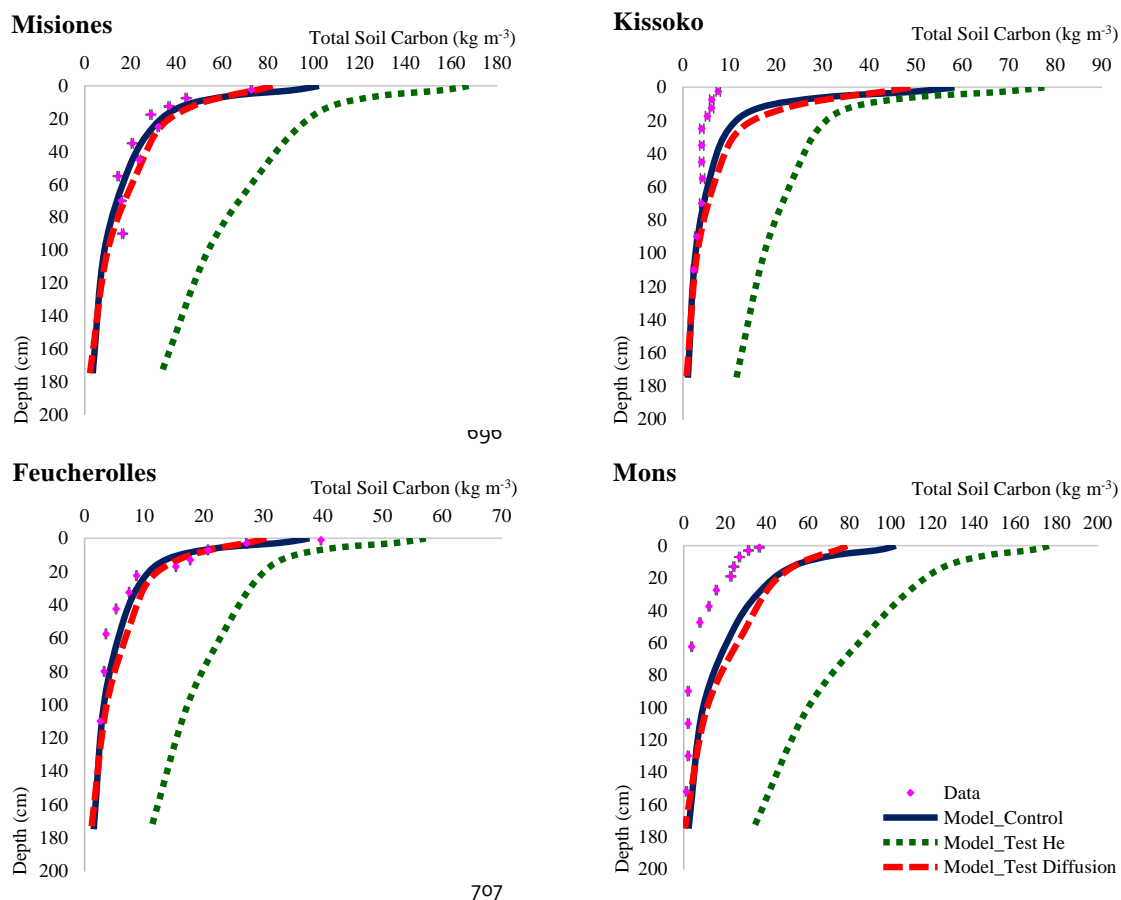
681



682

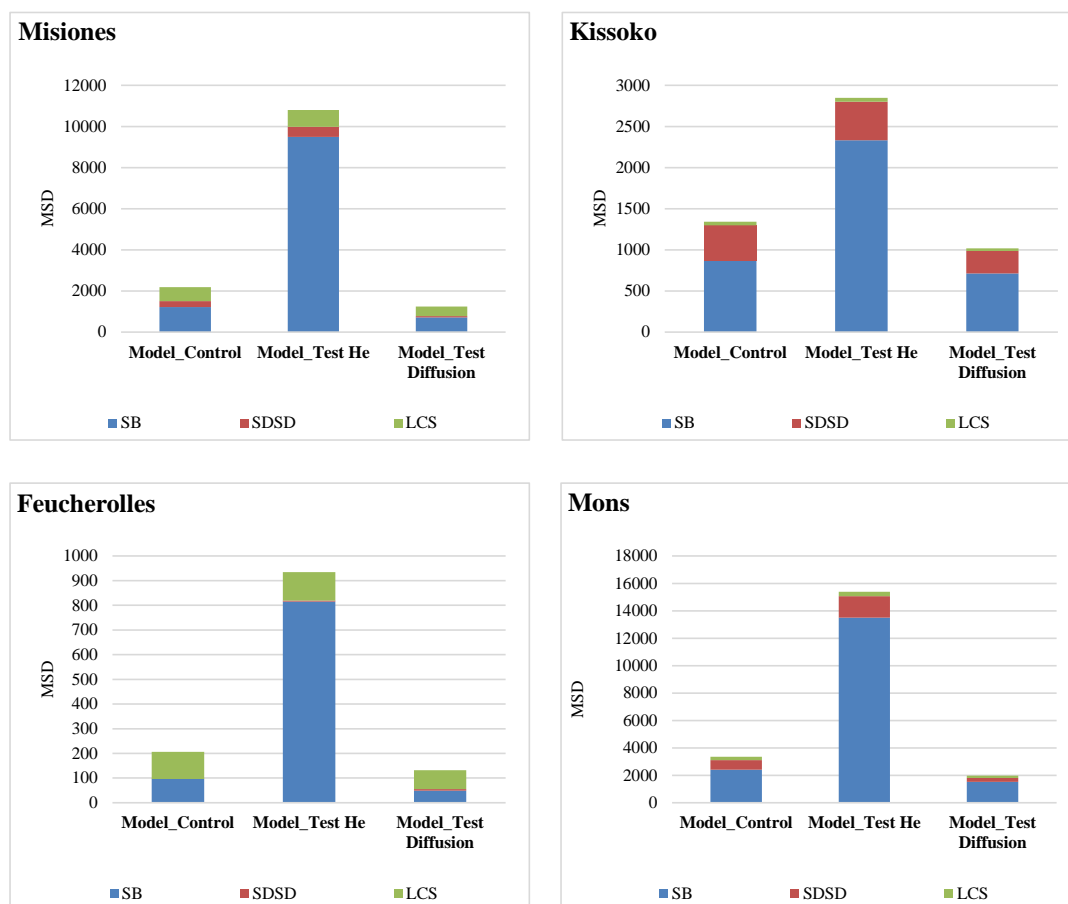
683

684 **Figure 2.** Evolution of the $F^{14}C$ of atmospheric CO_2 in Argentina, Congo and France (data
 685 from Hua et al. 2013)



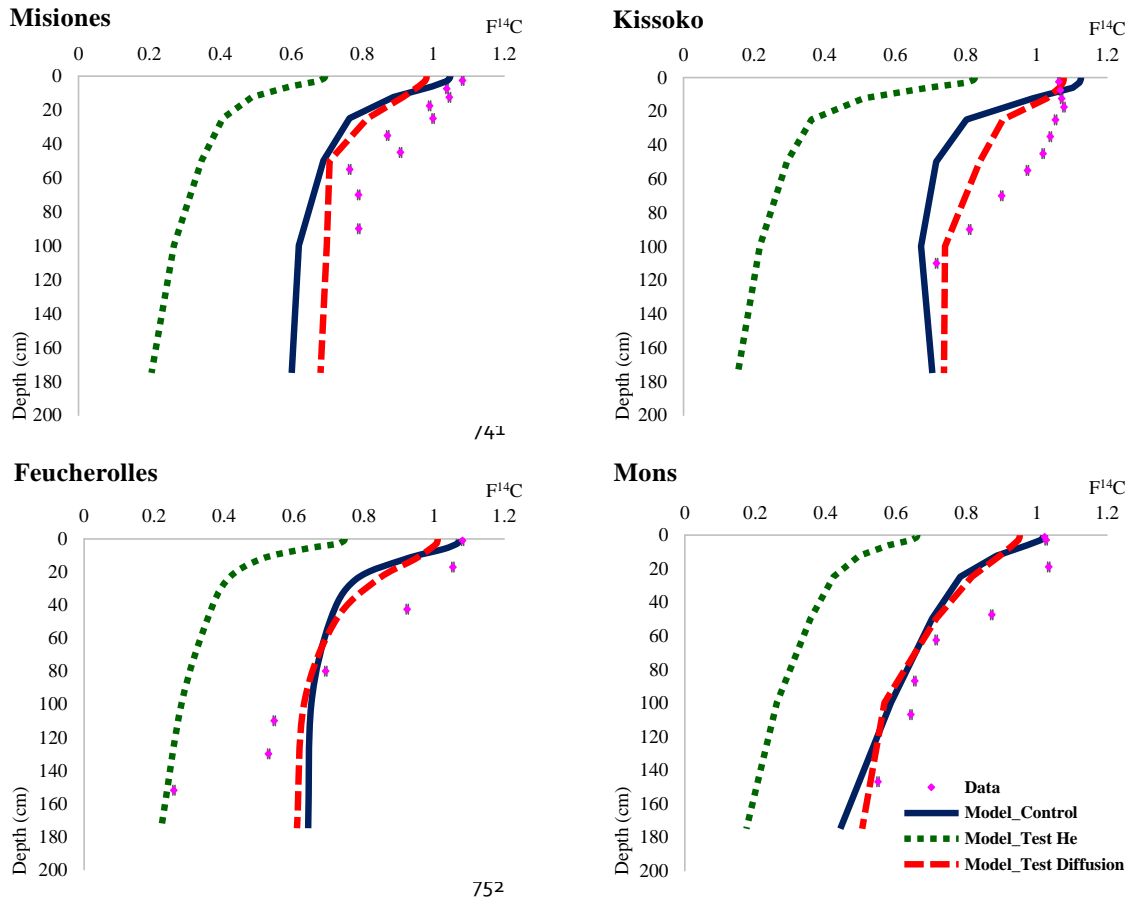
708 **Figure 3.** Total soil carbon (kg C m⁻³) according to the depth, for the four sites. The results of
709 the initial version of the model ORCHIDEE-SOM-¹⁴C (Model_Control) as well as those from
710 the version including the modification if the passive pool turnover rate and the slow-to-passive
711 flux revised according to (He et al., 2016) (Model_Test He) and diffusion varying according
712 to the depth (Model_Test Diffusion), are shown

713
714
715
716
717
718



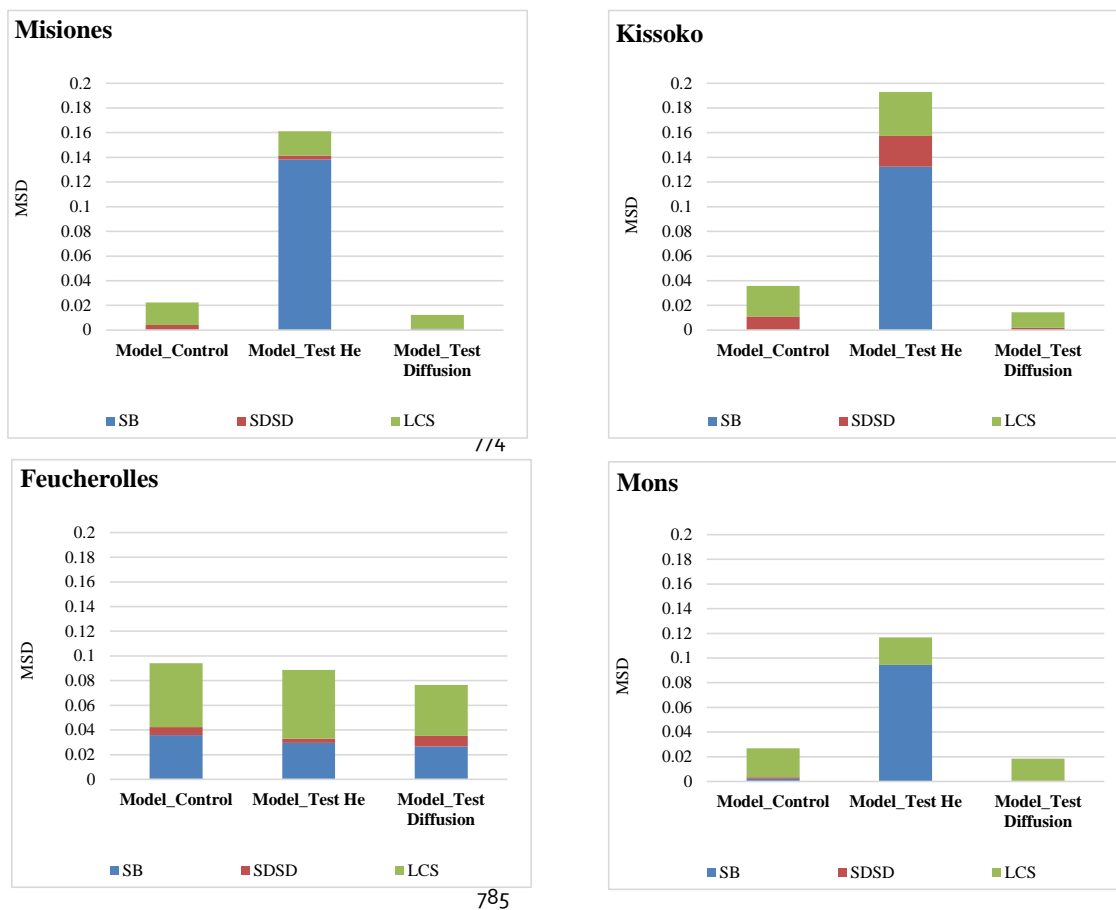
719 **Figure 4.** Mean Squared Deviation (MSD) and its components for total soil carbon (kg C m⁻³):
 720 lack of correlation weighted by the standard deviation (LCS), squared difference between
 721 standard deviations (SDSD) and the squared bias (SB). For the four sites, the results of the
 722 initial version of the model ORCHIDEE-SOM-¹⁴C (Model_Control as well as those from the
 723 version including the modification if the passive pool turnover rate and the slow-to-passive flux
 724 revised according to (He et al., 2016) (Model_Test He) and diffusion varying according to the
 725 depth (Model_Test Diffusion), are shown

726
 727
 728
 729
 730



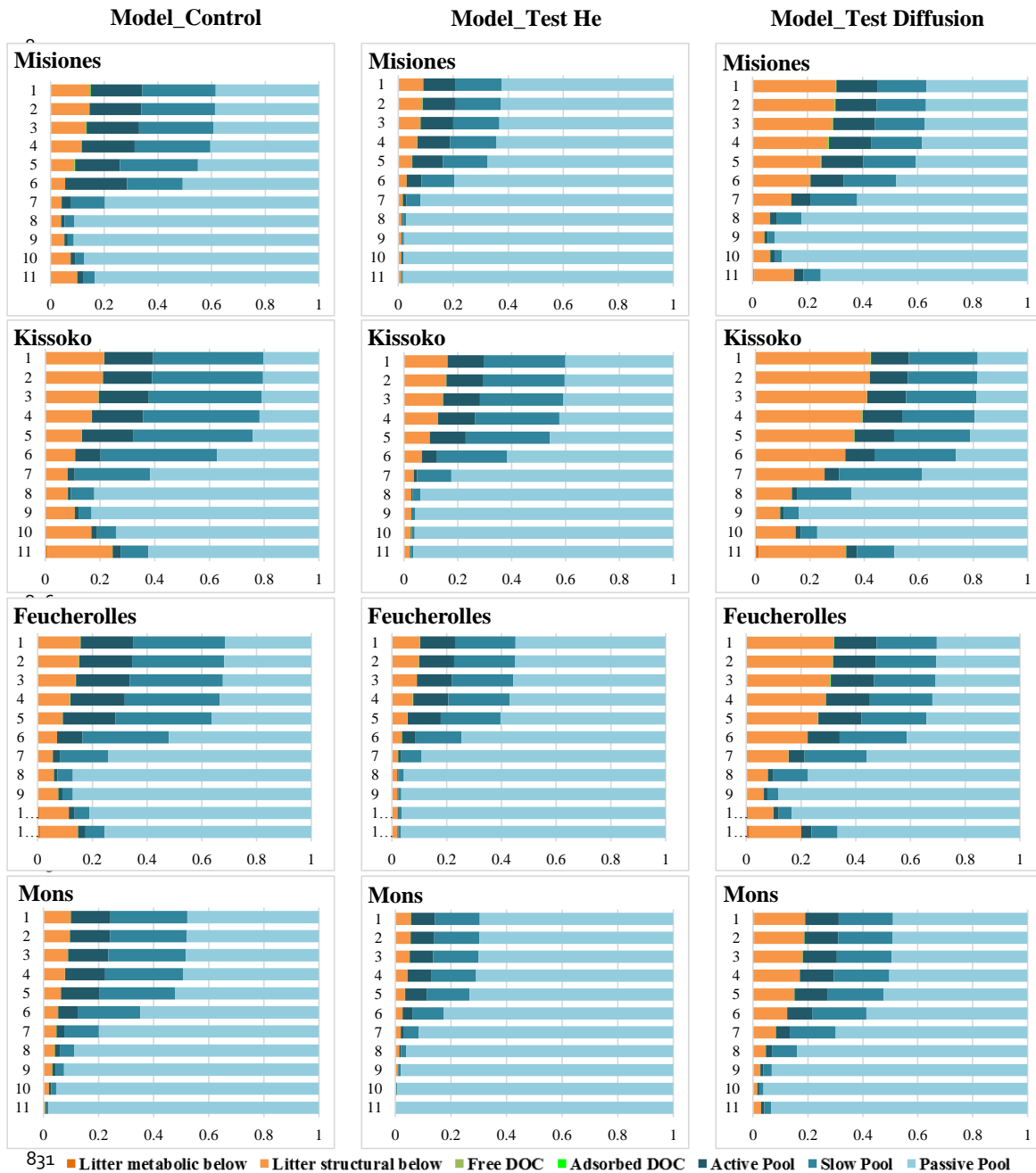
753 **Figure 5.** Modern fraction $F^{14}C$ according to the depth, for the four sites. The results of the
754 initial version of the model ORCHIDEE-SOM- ^{14}C (Model_Control) as well as those from the
755 version including the modification if the passive pool turnover rate and the slow-to-passive flux
756 revised according to He et al., (2016) (Model_Test He) and diffusion varying according to the
757 depth (Model_Test Diffusion), are shown

758
759
760
761
762
763



786 **Figure 6.** Mean Squared Deviation (MSD) and its components: lack of correlation weighted by
 787 the standard deviation (LCS), squared difference between standard deviations (SDDS) and the
 788 squared bias (SB). For the four sites, the results of the initial version of the model ORCHIDEE-
 789 SOM-¹⁴C (Model_Control) as well as those from the version including the modification if the
 790 passive pool turnover rate and the slow-to-passive flux revised according to He et al., (2016)
 791 (Model_Test He) and diffusion varying according to the depth (Model_Test Diffusion), are
 792 shown

793
 794
 795
 796
 797
 798
 799
 800



831 ■ Litter metabolic below ■ Litter structural below ■ Free DOC ■ Adsorbed DOC ■ Active Pool ■ Slow Pool ■ Passive Pool

832 **Figure 7.** Relative proportion of each of the soil carbon pools summing the total soil carbon at
 833 each soil layer. The results of the initial version of the model ORCHIDEE-SOM-¹⁴C
 834 (Model_Control, left pattern) as well as those from the version including the modification if the
 835 passive pool turnover rate and the slow-to-passive flux revised according to (He et al., 2016)
 836 (Model_Test He, pattern in the middle) and diffusion varying according to the depth
 837 (Model_Test Diffusion, right pattern), are shown